Strontium Hydroxyapatite and Strontium Carbonate as Templates for the Precipitation of Calcium-Phosphates in the Absence and Presence of Fluoride

Vanessa Sternitzke,[a,b,*] Markus Janousch,[c] Michèle B. Heeb,[a,b,d] Janet G. Hering,[a,b,d] and C. Annette Johnson[a]

[a] Eawag, Swiss Federal Institute of Aquatic Science and Technology, Ueberlandstrasse 133, 8600 Duebendorf, Switzerland

[b] Department of Environmental System Sciences, Institute of Biogeochemistry and Pollutant Dynamics, Swiss Federal Institute of Technology, ETH, Universitaetstrasse 8-22, 8092 Zurich, Switzerland

[c] Department of Large Research Facilities, Paul Scherrer Institute, PSI, 5232 Villigen, Switzerland

[d] School of Architecture Civil and Environmental Engineering, École Polytechnique Fédérale de Lausanne, EPFL, Station 2, 1015 Lausanne, Switzerland

*Corresponding author: Fraunhofer Institute for Mechanics of Materials, IWM, Walter-Huelse-Strasse 1, 06120 Halle (Saale), Germany; Phone: +49 345 5589 287, Fax: +49 345 5589 101; Email address: vanessa.sternitzke@iwmh.fraunhofer.de

Other e-mail addresses: markus.janousch@psi.ch, michele.heeb@epfl.ch, janet.hering@eawag.ch, annette.johnson@eawag.ch

ABSTRACT

The heterogeneous precipitation of calcium-phosphates on calcium hydroxyapatite ($Ca_{10}(PO_4)_6(OH)_2$ or HAP) in the presence and absence of fluoride is important in the formation of bone and teeth, protection against tooth decay, dental and skeletal fluorosis and defluoridation of drinking water.

Strontium hydroxyapatite ($Sr_{10}(PO_4)_6(OH)_2$ or SrHAP) and strontium carbonate ($SrCO_3$) were used as calcium-free seed templates in precipitation experiments conducted with varying initial calcium-to-phosphate (Ca/P) or calcium-to-phosphate-to-fluoride (Ca/P/F) ratios. Suspensions of SrHAP or $SrCO_3$ seed templates (which were calcium-limited for both templates and phosphate-limited in the case of $SrCO_3$) were reacted at pH 7.3 (25 °C) over 3 days. The resulting solids were examined with Scanning Transmission Electron Microscopy (STEM), X-ray Diffraction (XRD), Fourier Transform Infrared (FTIR), and X-ray Photoelectron Spectroscopy (XPS), X-ray Absorption Near Edge Structure (XANES), and Extended X-ray Absorption Fine Structure spectroscopy (EXAFS).

Calcium apatite was the predominant phase identified by all techniques independent of the added Ca/P ratios and of the presence of fluoride. It was not possible to make an unambiguous distinction between HAP and fluorapatite ($Ca_{10}(PO_4)_6F_2$, FAP). The apatite was calcium-deficient and probably contained some strontium.

Keywords:

A1. Characterization; A1. Crystal structure; A1. Impurities; A2. Seed crystals; B1. Phosphates

1. Introduction

The heterogeneous precipitation of calcium hydroxyapatite ($Ca_{10}(PO_4)_6(OH)_2$ or HAP) on bones and teeth (as templates) is a process of primary importance in vertebrate physiology [1]. The uptake of fluoride into HAP and the precipitation of fluorapatite ($Ca_{10}(PO_4)_6F_2$ or FAP) can protect teeth from caries, but at higher exposure, may lead to discoloration of teeth or even crippling bone weakness [2]. Medical and dental applications have motivated studies of HAP and FAP precipitated under highly-controlled and non-physiological conditions (e.g., hydrothermal synthesis [3, 4] or aerosol deposition onto titanium [5] or after calcination [6, 7]) complementing earlier studies on the precipitation of a variety of calcium phosphate solids [8-14]. In most studies, HAP and FAP (in the presence of dissolved fluoride, F) have been the thermodynamically-favored phases, but the formation of other calcium phosphate solids, particularly as intermediates, has also been reported depending on reaction time, solution conditions including the degree of super-saturation, initial calcium-to-phosphate (Ca/P) ratios, pH and ionic strength, temperature and surface area of HAP added as a seed template. Studies of F-substituted apatites have suggested that more crystalline apatites are formed at higher temperatures (over the range of 3-90 ^oC) [15, 16] and that fluorite (CaF_2) may be formed as an intermediate during FAP precipitation in aqueous solution [17]. Carbonate minerals have been used as either a seed or sacrificial template; overgrowth of octacalcium phosphate (OCP) has been observed on both calcite and mixed calcite-aragonite crystals [18] and complete dissolution of biogenic aragonite (cuttlefish bone) was observed in association with the formation of apatite [19], calcium phosphates [20] or fluoride-substituted hydroxyapatite [21].

Fluoride uptake by HAP and precipitation of FAP are also relevant to the defluoridation of drinking water [22-26]. Bone char (predominantly HAP) is being used for this purpose in rural Kenya; filters are amended with pellets containing calcium phosphates and calcite ($CaCO_3$) to improve performance [27]. The composition of pore fluids in the filters can be

highly variable due to variability in the composition of source waters, intermittent supply of water to the filters and physico-chemical reactions occurring in the filter bed.

Here, we use strontium carbonate ($SrCO_3$) and strontium hydroxyapatite ($Sr_{10}(PO_4)_6(OH)_2$ or SrHAP) as Ca-free templates for the precipitation of calcium phosphate phases. This study focused on distinguishing between calcium apatites and other calcium phosphate phases precipitated under ambient conditions (pH 7.3, 25 °C) after the addition of solutes with varying initial calcium-phosphate (Ca/P) ratios in the presence and absence of dissolved F. The intention of using Sr-based seed templates was to distinguish the newly-precipitated phases from the seed phases. Solutes were added in Ca/P ratios corresponding to the stoichiometry of various possible products: 1.0 for brushite ($CaHPO_4 \cdot 2H_2O$), 1.50 for β-tricalcium phosphate (β-$Ca_3(PO_4)_2$ or β-TCP), and 1.67 for HAP and FAP. When fluoride was added, the initial Ca/P/F ratios were either stoichiometric for FAP, F-limited for FAP or P-limited for FAP with excess Ca and F in the stoichiometric ratio for CaF_2. Solutes were added at concentrations relevant for filter systems used for defluoridation of drinking water. The composition of the solids produced after 3 d was characterized using Scanning Transmission Electron Microscopy (STEM), X-ray Photoelectron Spectroscopy (XPS), Fourier Transform Infrared Spectroscopy (FTIR), X-ray Absorption Near Edge Structure (XANES) and Extended X-ray Absorption Fine Structure (EXAFS) spectroscopy, and X-ray Diffraction (XRD). The stoichiometry of precipitated solids was calculated based on the removal of the constituent ions from solution.

2. Materials and Methods

2.1. Chemicals and Materials

All chemicals used (excluding FAP and SrHAP reference samples) were of at least "pro analysi" grade (p.a., from Merck and Fluka). Solutions were prepared in nanopure water (Barnstead NANOpure Diamond UV, resistivity > 18 MΩ-cm) in polyethylene vessels

washed with acid (0.65 % HNO_3) and rinsed at least 3 times with nanopure water. Solid reference samples were obtained from commercial suppliers (brushite and monetite ($CaHPO_4$) from Fluka, fluorite (CaF_2) from AlfaAesar, $SrCO_3$ from Merck, β-TCP from Cerros and HAP from Budenheim) or synthesized (SrHAP and FAP) as described elsewhere [28].

2.2. Batch experiments

Experiments were performed in duplicate in open systems (atmospheric pCO_2) at 25 ± 1 °C with 2g SrHAP or $SrCO_3$ in 1L nanopure water. Suspensions were stirred by a suspended magnetic stirrer to avoid sample grinding. Solution pH was controlled over the duration of the experiment at 7.3 ± 0.5 with 0.1 M HNO_3 and 0.1 M NaOH, using titration units as in [26, 28]. After dispersion for 10 min, dissolved Ca and PO_4 were added to the SrHAP/$SrCO_3$ suspensions from 0.5 M $Ca(NO_3)_2$, 0.3 M $NaH_2PO_4 \cdot H_2O$, 0.3 M Na_2HPO_4, and 0.4 M NaF stock solutions (accommodating changes in volume due to pH-adjustment and sampling prior to solute addition) to achieve target initial solute concentrations (1-6 mM Ca, 2-5 mM PO_4, 0-3 mM F, Table 1). After 3 d, solids were collected on cellulose-nitrate filters (0.45 µm, Sartorius), air-dried and stored at room temperature for further analysis. Filtrates for solute analysis were collected by filtration through nylon filters (0.2 µm, PALL) and analyzed for major cations (Na, Ca and Sr) and anions (chloride and phosphate) as well as for total dissolved inorganic carbon as described previously [26]. Reported concentrations were corrected to account for dilution during pH adjustment.

2.3. Solid characterization

Analyses by XPS, XRD and FTIR were performed for all precipitates and for the reference samples HAP, FAP, SrHAP, $SrCO_3$ and CaF_2 as described previously [26] except for modification of the FTIR analysis parameters as follows: spectra recording velocity 10 kHz; filter 1.2 kHz, undersampling ratio (UDR) 2, resolution 2 cm^{-1}, aperture 0.25 cm^{-1} and sensitivity 16 [–]. All FTIR data were normalized to the baseline. For STEM analysis of the

precipitated sample HAP_SrHAP, about 20 mg of well-ground, air-dried sample was suspended in approximately 50 mL ethanol, sonicated in a water bath (Bioblock Scientific) for 2 min and centrifuged (UniCen MR, Herolab) at 4300 rpm for 10 min to remove large aggregates. Two drops of the supernatant were deposited on a TEM grid (Cu/holey carbon-coated; Okenshoji Co., Ltd). The microscope (Hitachi HD 2700Cs) was operated with an acceleration voltage of 200 kV in a high resolution mode. The solids were localized using a High-Angle Annular Dark Field (HAADF) detector and analyzed with an Energy Dispersive X-Ray (EDX) system (EDAX). The data was evaluated using EDAX Genesis V6.2 and Matlab. X-ray absorption spectroscopy was performed on the X07MB PHOENIX beamline at the Swiss Light Source (SLS, Paul Scherrer Institute PSI, Switzerland). About 70 mg of well-ground, air-dried samples were pressed into discs of 10 mm diameter; the references (HAP, FAP, CaF_2, β-TCP, brushite and monetite) were diluted with cellulose powder to obtain 3 % Ca in each sample. The pressed samples were glued with double-sided sticky carbon tape onto a copper sample plate, which was set at an angle of 45° with respect to the incoming beam and the fluorescence detector. The spectra were collected in an energy range between 4000 and 4760 eV (Ca K-edge) with an energy step size of 2 eV in the pre-edge, 0.25 eV in the XANES and an increasing step size up to 5 eV in the EXAFS region. A dwell time of up to 6 s was applied for each point. A Si (111) double crystal monochromator provided an energy resolution of about 0.6 eV. The beam size was 1 x 1 mm² and the measurements were performed at a temperature of 25°C under vacuum with a residual pressure of about 5×10^{-5} mbar. The fluorescence signal was detected by a four-element silicon drift detector and corrected for dead-time effects. A calibration of the X-ray energy used the first inflection point of a Ti K-edge spectrum and was set to 4966 eV. The data were normalized to the incoming flux by recording the total electron yield of a 0.5 µm thick polyethylene foil covered by a 50 nm thick Ni-layer. The IFEFFIT package was used for analysis [29]. A linear pre-

edge was subtracted from the data, which were then normalized to a unit step by 3rd polynominal fit to the post-edge data.

3. Results and discussion

The formation of calcium-phosphate phases in heterogeneous suspensions containing Ca-free seed templates of SrHAP or $SrCO_3$ was examined at varying Ca/P ratios in the absence and presence of F. Although Ca was supplied only by addition of solutes to the seed template suspensions, dissolution of $SrCO_3$ and SrHAP released Sr to the solution [28], which can be re-incorporated into newly-formed calcium phosphate solids [30-34]. In SrHAP suspensions, dissolution also released phosphate to the solution, thus Ca/P ratios were fully controlled only in the $SrCO_3$ suspensions. Dissolution of the seed templates during the 10-min pre-equilibration was accounted for in calculating saturation indices for various solids. In all cases, HAP and/or FAP in the F-amended experiments were the most thermodynamically-favorable solids but some systems were also over-saturated with respect to brushite, β-TCP, OCP and CaF_2 [28]. The calculation of saturation indices for fluoridated SrHAP and SrF_2 was not possible due to lack of published solubility values.

3.1. Incorporation of ions from solution into solid phases

The association of Ca with the SrHAP seed template is clearly illustrated in X-ray intensity maps obtained with STEM (Figure 1). The signals of Sr, P and O can be attributed mainly to the residual SrHAP seed template. The intensity of the Ca signal is relatively weak consistent with calcium-phosphate precipitation corresponding to a maximum of 10 % by weight relative to the original seed. Adsorption of Ca onto the SrHAP seed or Ca substitution within the SrHAP crystal structure could also contribute to the observed signal. Normalizing the Ca signal to the Sr intensities shows a heterogeneous distribution on the particle aggregate and does not necessarily coincide with the P/Sr or O/Sr ratios and Ca intensities. These

findings further support an inhomogeneous distribution of the calcium-phosphate precipitates, but also a removal of Sr from the seed.

Similarly, clear signatures of Ca uptake were observed with XPS in all reacted samples (Table 2) at binding energies consistent with HAP and/or FAP [35]. Neither of the unreacted references SrHAP and $SrCO_3$ exhibited any Ca(2p) signal. The Ca signals in reacted samples were significantly (16-49 %) lower than those of the HAP/FAP references; the Sr signals were also lower than those of the SrHAP/$SrCO_3$ references. The (Sr + Ca)/P ratios of all SrHAP-based solids were between 1.62 and 1.94, whereas the ratio for the reference HAP (1.43) was lower than stoichiometric (1.67) and that of the reference SrHAP (1.99) was higher. Since XPS penetrates to a depth of about 5 nm and averages over an area of approximately 0.02 mm^2, this may reflect sampling into the bulk of the seed template coated with Ca- or Ca/Sr surface precipitates or across neighboring particles with different composition. (Please note, although every attempt was made to homogeneously distribute each sample it is possible that the precipitates, clustered on the seeds, were more enriched in one sample than in the other, affecting XPS intensities.) With the P-free $SrCO_3$ seed template, P(2s) signals consistent with HAP/FAP were also observed at lower intensities than in the reference solids. A weak P signal in the reference $SrCO_3$ is attributed to contamination during sample preparation. Samples precipitated in the presence of F exhibited a F(1s) signal but this could not be interpreted quantitatively because of the observed signal for F (0.43 ± 0.11 atm%; n = 6) in nominally F-free seeding templates and solids obtained from F-free suspensions. Potential ion incorporation (e.g. of Na) was not observed, and the carbonate C content for the SrHAP-based precipitates was less than 1 atm%.

Uptake of phosphate from solution is also demonstrated by the FTIR spectra of precipitates formed in the presence of F using the $SrCO_3$ seed template (Figure 2). Coincident with the observed decrease in dissolved phosphate (and Ca) concentrations, the intensity of

the carbonate-associated absorbance (i.e., at 1435 cm^{-1}) decreased and the absorbance attributable to phosphate groups in an apatite environment (i.e., at 1027 cm^{-1}) increased. Comparable spectra have been reported elsewhere [6]. The absorbance attributed to phosphate in FAP was slightly shifted to higher wavenumbers compared to those observed for HAP (1022 cm^{-1}) and SrHAP (1006 cm^{-1}) (Figure 2 and S2) and phosphate related peak positions of F-containing precipitates in $SrCO_3$-based systems were more similar to FAP than HAP. The shift to higher wavenumbers for FAP contrasts with observations in a study in which F-substituted HAP was prepared by the cyclic pH method and subsequently calcined [36]. In this study, identical absorbances (at 1018 cm^{-1}) for HAP and F-substituted HAP were observed with a shift to higher wavenumbers in the absorbance (to 1021 cm^{-1}) only after calcining of F-substituted HAP. (Note, however, that IR positions of 1027 and 1034 cm^{-1} have been reported for the ν_3 PO_4-bands of HAP standard reference material [37, 38].) No shifts of the phosphate-assigned peaks were observed for the F-containing SrHAP-based systems as would have been expected if F was substituted for hydroxyl groups within SrHAP. No indications of SrF_2 formation were observed for either SrHAP- or $SrCO_3$-based systems.

3.2. Local environment of Ca in precipitated solids and identification of precipitated phases

The local environment of Ca was interrogated with X-ray Absorption Spectroscopy (XAS). For all precipitates with both SrHAP and $SrCO_3$ seed templates, XANES spectra were consistent with the references of HAP/FAP (Figure 3), though they exhibited slight differences at the white line (main peak of the spectra). In comparison to the reference HAP, the precipitated samples did not exhibit a dip between 4049.9 and 4051.5 eV (see Figure 3b).

The white line dip at 4050.5 eV is caused by two different kinds of Ca atoms within the HAP and FAP crystal structure, which are coordinated in hexagonal shaped channels formed by PO_4 groups. One unit cell consists of four Ca ions (Ca I) located outside the PO_4 channel, while six Ca ions (Ca II) are located inside the PO_4 channel and are coordinated to two OH

(HAP) or to two F ions (FAP) [39]. The white line peak at 4049.9 eV associated with Ca I is more intense than the peak at 4051.5 eV associated with Ca II. The peaks are separated by a slight dip at 4050.5 eV. Thus, the absence of this dip is indicative of either a Ca-deficient apatite of low crystallinity or of the presence of another calcium phase.

The crystal structures of both, brushite and β-TCP, contain one type of Ca atoms, which results in a single and round white line peak (Figure 3c), while OCP exhibits a plateau-like shape [40]. The distinctly different appearance of the CaF_2 spectra is a consequence of its cubic structure and is not evident for any of the precipitated samples.

In the EXAFS spectra, characteristic features of HAP/FAP assigned to the first O shell surrounding the two Ca atoms (Ca I and Ca II) were observed at 1.8 Å (Figure 4). The features above 2.5 Å are attributed to mixtures of single scattering from P and Ca accompanied by multiple scattering involving mainly O and P atoms, thus are difficult to interpret. While the EXAFS spectrum shown for HAP agrees with that previously reported [41], the spectra of the precipitates between 3.0 and 4.0 Å seem to be a mixture of the single symmetrical peak of HAP and one broad feature of FAP. In contrast to the single symmetrical peak observed in the HAP spectrum, a broader feature with a noticeable downward slope from 2.8-3.2 Å is observed for all SrHAP-based precipitates formed in the absence of F, except β-TCP_SrHAP (Figure 4a). The broader feature, but with an upward slope or with a flat feature as β-TCP_SrHAP, is observed for the precipitates formed in presence of F (i.e., precipitated on both SrHAP and $SrCO_3$ templates). Possibly this distinct difference to the HAP reference is a result of phase synthesis, since the HAP reference was a commercial product heated to about 200°C, unlike the FAP reference and the precipitated samples that were air-dried solids of relatively low crystallinity. It is notable that the spectra of all the precipitates exhibited increased intensity of the feature at 1.3 Å, which appears only as a shoulder in the (Sr-free) HAP and FAP references. This feature may be attributed to changes in the scattering path

length of the photoelectron of the O shell by the incorporation of Sr. Data evaluation for fluoridated SrHAP or SrF_2 was not possible, as analyses were performed on the Ca-K-edge and not on the Sr-K-edge.

XRD spectra of all precipitates showed a strong signature of the templates consistent with previously reported spectra of SrHAP [42] and $SrCO_3$ [43]. For precipitates formed on the SrHAP template, a weak peak was observed at 25.8^o 2θ (Figure 5), which is consistent with the (0 0 2) reflection of HAP [42], also reported at 25.9^o 2θ [44, 45]. The offset between the reflections observed in the newly-formed HAP as compared with the template SrHAP is associated with the smaller size of the Ca cation. The crystal structure of SrHAP (a=b: 9.745 Å and c: 7.265 Å) [42] is similar to that of HAP (a=b: 9.4166 Å and c: 6.8745 Å) [44] with the slightly larger unit cell size of SrHAP corresponding to the difference in ionic radii (Ca: 11.4 Å; Sr: 13.2 Å) [46]. Although other Ca-phosphate solids (i.e., β-TCP or OCP) could also account for the peak at 25.8^o 2θ [47-49], stronger reflections that would have been expected for these solids (and also for brushite [50]) were not observed [28].

For precipitates formed on the $SrCO_3$ template, this region of the diffractogram is obscured by the $SrCO_3$ (0 2 1) reflection at 31.6^o 2θ [43]. The appearance of a shoulder adjacent to this peak was observed in all $SrCO_3$-based precipitates (Figure S3) consistent with the (1 1 2), (2 1 1) and (3 0 0) reflections of HAP and FAP [7, 16].

Ratios of Ca/P in the precipitates were calculated from the observed decrease in the dissolved concentrations of the constituent ions (Table 1). The amount of solutes released by partial dissolution of the seed templates during the 10 min pre-equilibration was accounted for in this calculation, but further dissolution of the seed template during the precipitation phase of the experiment was neglected. Observed ratios ranged from 1.16 to 1.90 with the highest ratios observed in the presence of F, particularly for the systems that were (nominally) phosphate-limited for FAP. Note that this applies strictly only for the $SrCO_3$ seed template,

since continuing dissolution of the SrHAP template would supply additional phosphate to solution. Ratios exceeding the stoichiometric value for HAP/FAP of 1.67 suggest the formation of an additional Ca-containing phase such as CaF_2. Ratios below the stoichiometric value (i.e. for FAP_$SrCO_3$, FAP-HAP_$SrCO_3$, FAP-HAP_SrHAP) have been observed in previous studies and have been attributed to the formation of Ca-deficient HAP or F-substituted HAP [6, 51-53], formation of amorphous calcium phosphate as an intermediate [54] or precipitation of brushite [23, 55]. In our experiments, such ratios could also result from substitution of Sr for Ca, which has been previously reported for phosphate solids [30-34]. A rapid decrease in dissolved Sr (from 0.24 to 0.17 mM) was observed subsequent after addition of the stock solutions, supporting re-precipitation of Sr-containing phases accounting for approximately 5.8 mg (0.25 wt%) SrHAP. Measurement of dissolved Sr concentrations in experiments conducted with the $SrCO_3$ seed template was indicative of continuing dissolution (from 0.09 to 1.59 mM) over the course of the experiment [28]. An increased consumption of pH-adjusting acid upon the addition of F to the pre-conditioned suspensions was not observed [28], which would indicate for a substitution of hydroxyl groups by F within SrHAP.

3.3. Comparison of interrogation methods

The results of all methods for interrogating the precipitates formed on SrHAP and $SrCO_3$ seed templates were consistent with the formation of calcium apatite. These results were independent of the sample area or whether it was a bulk XRD (1.0 cm^2), FTIR (2.0 mm^2), and XAS (1.0 mm^2) or surface analysis like XPS (0.02 mm^2). However, a co-occurrence of fluoridated SrHAP cannot be entirely excluded. The small amount of newly-formed precipitates (roughly 10 % by weight of the starting seed template), their poor crystallinity (indicated by XRD, STEM and XAS) and apparent Ca-deficiency (suggested by XAS and Ca/P ratios) made it difficult to distinguish between HAP and FAP, to definitively exclude solids such as brushite, OCP or β-TCP or to exclude entirely the potential incorporation of

sodium or carbonate. Substitution of Sr for Ca in newly-formed precipitates was indicated by observed Ca/P ratios, by XPS and XAS.

4. Conclusion

The use of SrHAP and $SrCO_3$ as seed templates allowed the investigation of precipitates that formed upon addition of solutes (calcium, phosphate and fluoride). In particular, XAS spectra could be obtained at the Ca K-edge with Ca-free seed templates.

The solids were collected and examined after 3 d. Observations from multiple techniques were consistent with the presence of the thermodynamically-favored phases HAP and FAP as poorly-crystalline, probably Ca-deficient phases, which formed as aggregated solids with the seed templates and not as homogenous surface coatings. Collection and analysis at shorter equilibration times might allow the identification of intermediates that have been suggested in previous studies [9, 11, 12, 56, 57]. The principle limitation of this study, however, is the dissolution of the seed templates, which releases Sr into solution, particularly for $SrCO_3$, as well as phosphate for the SrHAP template. The formation of fluoridated SrHAP has also to be considered, particularly, since the systems did not achieve equilibrium. Since the seed template appeared to have little influence on the nature of the precipitate, a more insoluble solid could be substituted as a template for heterogeneous precipitation in further studies.

Acknowledgments

This work was supported by funding from the Swiss National Science Foundation (200021-117992). XAS were performed at the Paul Scherrer Institute (X07MB PHOENIX beamline) at the Swiss Light Source. For support of the various analytical techniques, we thank the following colleagues: XPS: E. Lewin (Empa), STEM: R. Kaegi (Eawag), FTIR: S. Hug (Eawag), XRD: G. Lesaout (Empa) and S. Yoon (Empa). We thank H. Moench for assistance in the laboratory and two anonymous reviewers for constructive feedback.

Supporting Information

Supplemental data (Figures S1-S3) are available at www.sciencedirect.com.

References

[1] S.V. Dorozhkin, M. Epple, Biological and Medical Significance of Calcium Phosphates, Angew. Chem., Int. Ed., 41 (2002) 3130-3146.
[2] J. Fawell, K. Bailey, J. Chilton, E. Dahi, L. Fewtrell, Y. Magara, Fluoride in Drinking-water, in, WHO, 2001;
http://www.who.int/water_sanitation_health/publications/fluoride_drinking_water_full.pdf, accessed on Sept. 4,
2008
[3] A.J. Nathanael, D. Mangalaraj, S.I. Hong, Y. Masuda, Y.H. Rhee, H.W. Kim, Influence of fluorine substitution on the morphology and structure of hydroxyapatite nanocrystals prepared by hydrothermal method, Mater. Chem. Phys., 137 (2013) 967-976.
[4] L. Montazeri, J. Javadpour, M.A. Shokrgozar, S. Bonakdar, S. Javadian, Hydrothermal synthesis and characterization of hydroxyapatite and fluorhydroxyapatite nano-size powders, Biomed. Mater., 5 (4), 2010, 045004.
[5] B.D. Hahn, Y.L. Cho, D.S. Park, J.J. Choi, J. Ryu, J.W. Kim, C.W. Ahn, C. Park, H.E. Kim, S.G. Kim, Effect of fluorine addition on the biological performance of hydroxyapatite coatings on Ti by aerosol deposition, J. Biomater. Appl., 27 (2013) 587-594.
[6] L.M. Rodriguez-Lorenzo, J.N. Hart, K.A. Gross, Influence of fluorine in the synthesis of apatites. Synthesis of solid solutions of hydroxy-fluorapatite, Biomaterials, 24 (2003) 3777-3785.
[7] M. Wei, J.H. Evans, T. Bostrom, L. Grondahl, Synthesis and characterization of hydroxyapatite, fluoride-substituted hydroxyapatite and fluorapatite, J. Mater. Sci-Mater. Med., 14 (2003) 311-320.
[8] Z. Amjad, P.G. Koutsoukos, G.H. Nancollas, The crystallization of fluoroapatite. A constant composition study, J. Colloid Interface Sci., 82 (1981) 394-400.
[9] J.P. Barone, G.H. Nancollas, The seeded growth of calcium phosphates. The effect of solid/solution ratio in controlling the nature of the growth phase, J. Colloid Interface Sci., 62 (1977) 421-431.
[10] J.P. Barone, G.H. Nancollas, The Growth of Calcium Phosphates on Hydroxyapatite Crystals. The Effect of Fluoride and Phosphonate, J. Dent. Res., 57 (1978) 735-742.
[11] J.P. Barone, G.H. Nancollas, The Seeded Growth of Calcium Phosphates. The Kinetics of Growth of Dicalcium Phosphate Dihydrate on Enamel, Dentin, and Calculus, J. Dent. Res., 57 (1978) 153-161.
[12] P. Koutsoukos, Z. Amjad, M.B. Tomson, G.H. Nancollas, Crystallization of calcium phosphates. A constant composition study, J. Am. Chem. Soc., 102 (1980) 1553-1557.
[13] G.H. Nancollas, B. Tomazic, Growth of calcium phosphate on hydroxyapatite crystals. Effect of supersaturation and ionic medium, J. Phys. Chem., 78 (1974) 2218-2225.
[14] B. Tomazik•, G.H. Nancollas, The seeded growth of calcium phosphates. Surface characterization and the effect of seed material, J. Colloid Interface Sci., 50 (1975) 451-461.
[15] L.J. Jha, S.M. Best, J.C. Knowles, I. Rehman, J.D. Santos, W. Bonfield, Preparation and characterization of fluoride-substituted apatites, J. Mater. Sci-Mater. M., 8 (1997) 185-191.
[16] Q.X. Zhu, W.H. Jiang, H.D. Wang, C. Shao, Investigation on Preparation Factors for Fluorhydroxyapatite by an Aqueous Precipitation Method, J. Inorg. Mater., 26 (2011) 1335-1340.

[17] M. Fulmer, P.W. Brown, Low-temperature formation of fluorapatite in aqueous-solution, J. Am. Ceram. Soc., 75 (1992) 3401-3407.
[18] S. Rokidi, C. Combes, P.G. Koutsoukos, The Calcium Phosphate-Calcium Carbonate System: Growth of Octacalcium Phosphate on Calcium Carbonates, Cryst. Growth Des., 11 (2011) 1683-1688.
[19] A. Kasioptas, T. Geisler, C.V. Putnis, C. Perdikouri, A. Putnis, Crystal growth of apatite by replacement of an aragonite precursor, J. Cryst. Growth, 312 (2010) 2431-2440.
[20] A. Dutta, S. Fermani, S.A. Tekalur, A. Vanderberg, G. Falini, Calcium phosphate scaffold from biogenic calcium carbonate by fast ambient condition reactions, J. Cryst. Growth, 336 (2011) 50-55.
[21] S. Kannan, J.H.G. Rocha, S. Agathopoulos, J.M.F. Ferreira, Fluorine-substituted hydroxyapatite scaffolds hydrothermally grown from aragonitic cuttlefish bones, Acta Biomater. , 3 (2007) 243-249.
[22] H.V. Smith, M.C. Smith, Bone contact removes fluorine, Water Works Eng., 11 (1927) 1600-1603.
[23] M.J. Larsen, E.I.F. Pearce, Partial defluoridation of Drinking Water Using Fluorapatite Precipitation, Caries Res., 26 (1992) 22-28.
[24] M.J. Larsen, E.I.F. Pearce, Defluoridation of Drinking Water by Boiling with Brushite and Calcite, Caries Res., 36 (2002) 341-346.
[25] M.J. Larsen, E.I.F. Pearce, S.J. Jensen, Defluoridation of Water at High pH with Use of Brushite, Calcium Hydroxide, and Bone Char, J. Dent. Res., 72 (1993) 1519-1525.
[26] V. Sternitzke, R. Kaegi, J.-N. Audinot, E. Lewin, J.G. Hering, C.A. Johnson, Uptake of Fluoride from Aqueous Solution on Nano-Sized Hydroxyapatite: Examination of a Fluoridated Surface Layer, Environ. Sci. Technol., 46 (2012) 802-809.
[27] H. Korir, K. Mueller, L. Korir, J. Kubai, E. Wanja, N. Wanjiku, J. Waweru, M. Mattle, L. Osterwalder, C.A. Johnson, The development of bone char-based filters for the removal of fluoride from drinking water, 34th WEDC International Conference, Addis Ababa, Ethiopia, 2009.
[28] V. Sternitzke, Optimization of co-precipitation processes in apatite-based filter materials for the removal of fluoride from drinking water, Swiss Federal Institute of Technology (ETH), Zurich, Switzerland, 2012.
[29] B. Ravel, M. Newville, ATHENA, ARTEMIS, HEPHAESTUS: data analysis for X-ray absorption spectroscopy using IFEFFIT, J. Synchrotron Rad., 12 (2005) 537-541.
[30] E. Rokita, C. Hermes, H.F. Nolting, J. Ryczek, Substitution of calcium by strontium within selected calcium phosphates, J. Cryst. Growth, 130 (1993) 543-552.
[31] J. Christoffersen, M.R. Christoffersen, N. Kolthoff, O. Bärenholdt, Effects of strontium ions on growth and dissolution of hydroxyapatite and on bone mineral detection, Bone, 20 (1997) 47-54.
[32] S. Rokidi, P.G. Koutsoukos, Crystal growth of calcium phosphates from aqueous solutions in the presence of strontium, Chem. Eng. Sci., 77 (2012) 157-164.
[33] Z.Y. Li, W.M. Lam, C. Yang, B. Xu, G.X. Ni, S.A. Abbah, K.M.C. Cheung, K.D.K. Luk, W.W. Lu, Chemical composition, crystal size and lattice structural changes after incorporation of strontium into biomimetic apatite, Biomaterials, 28 (2007) 1452-1460.
[34] H.B. Pan, Z.Y. Li, W.M. Lam, J.C. Wong, B.W. Darvell, K.D.K. Luk, W.W. Lu, Solubility of strontium-substituted apatite by solid titration, Acta Biomater., 5 (2009) 1678-1685.
[35] S. Chander, D.W. Fuerstenau, An XPS study of the flouride uptake by hydroxyapatite, Colloids Surface, 13 (1985) 137-144.

[36] L. Rintoul, E. Wentrup-Byrne, S. Suzuki, L. Grondahl, FT-IR spectroscopy of fluoro-substituted hydroxyapatite: strengths and limitations, J. Mater. Sci.-Mater. Med., 18 (2007) 1701-1709.
[37] B.O. Fowler, E.C. Moreno, W.E. Brown, Infra-red spectra of hydroxyapatite, octacalcium phosphate and pyrolysed octacalcium phosphate, Arch. Oral Biol., 11 (1966) 477-492.
[38] M. Markovic, B.O. Fowler, M.S. Tung, Preparation and comprehensive characterization of a calcium hydroxyapatite reference material, J. Res. Natl. Inst. Stand. Technol., 109 (2004) 553-568.
[39] J. Elliott, Structure and Chemistry of the Apatites and Other Calcium Orthophosphates., In *Studies in Inorganic Chemistry*, 18; Elsevier Science, Amsterdam, Netherlands, 1994.
[40] D. Eichert, M. Salomé, M. Banu, J. Susini, C. Rey, Preliminary characterization of calcium chemical environment in apatitic and non-apatitic calcium phosphates of biological interest by X-ray absorption spectroscopy, Spectrochim. Acta, Part B, 60 (2005) 850-858.
[41] J.E. Harries, D.W.L. Hukins, Analysis of the EXAFS spectrum of hydroxyapatite, J. Phys. C: Solid State Phys., 19 (1986) 6859-6872.
[42] K. Sudarsanan, R.A. Young, Structure of strontium hydroxide phosphate, Sr5(PO4)3OH, Acta Crystallogr., 28 (1972) 3668-3670.
[43] D. Jarosch, G. Heger, Neutron diffraction investigation of strontianite, SrCO3, Bull. Mineral., 111 (1988) 139-142.
[44] J.M. Hughes, M. Cameron, K.D. Crowley, Structural variations in natural F, OH, and Cl apatites, Am. Mineral., 74 (1989) 870-876.
[45] A.T. Saenger, W.F. Kuhs, Structural disorder in hydroxyapatite, Z. Kristallogr., 199 (1992) 123-148.
[46] R.D. Shannon, Revised effective ionic radii and systematic studies of interatomic distances in halides and chalcogenides, Acta Crystallogr., 32 (1976) 751-767.
[47] W.E. Brown, Octacalcium Phosphate and Hydroxyapatite: Crystal Structure of Octacalcium Phosphate, Nature, 196 (1962) 1048-1050.
[48] P.A. Henning, E. Adolfsson, J. Grins, The chalcogenide phosphate apatites Ca10(PO4)6S, Sr10(PO4)6S, Ba10(PO4)6S and Ca10(PO4)6Se, Z. Kristallogr., 215 (2000) 226-230.
[49] M. Yashima, A. Sakai, T. Kamiyama, A. Hoshikawa, Crystal structure analysis of beta-tricalcium phosphate Ca3(PO4)2 by neutron powder diffraction, J. Solid State Chem., 175 (2003) 272-277.
[50] N.A. Curry, D.W. Jones, Crystal structure of brushite, calcium hydrogen orthophosphate dihydrate: a neutron-diffraction investigation, J. Chem. Soc. A.: Inorganic, Physical, Theoretical, (1971) 3725-3729.
[51] Y. Fang, D.K. Agrawal, D.M. Roy, Thermal stability of synthetic hydroxyapatite, in: P.W. Brown, B. Constantz (Eds.) Hydroxyapatite and Related Materials, CRC Press, Boca Raton, FL, 1994, pp. 269-282.
[52] L.M. Rodriguez-Lorenzo, J.N. Hart, K.A. Gross, Structural and chemical analysis of well-crystallized hydroxyfluorapatites, J. Phys. Chem. B, 107 (2003) 8316-8320.
[53] S. Matsuya, Y. Matsuya, S. Takagi, L.C. Chow, Effect of fluoride on apatite formation from Ca-4(PO4)(2)O in 0.1 mol L-1 KH2PO4, J. Mater. Sci.-Mater. M., 9 (1998) 325-331.
[54] E.D. Eanes, I.H. Gillessen, A.S. Posner, Intermediate States in the Precipitation of Hydroxyapatite, Nature, 208 (1965) 365-367.
[55] E.I. Pearce, M.J. Larsen, Defluoridation of Drinking Water by Co-Precipitation with Apatite, Caries Res., 27 (1993) 378-386.

[56] J.L. Meyer, E.D. Eanes, A thermodynamic analysis of the amorphous to crystalline calcium phosphate transformation, Calcif Tissue Int, 25 (1978) 59-68.
[57] Z. Zyman, D. Rokhmistrov, V. Glushko, Structural changes in precipitates and cell model for the conversion of amorphous calcium phosphate to hydroxyapatite during the initial stage of precipitation, J. Cryst. Growth, 353 (2012) 5-11.

Figure captions

Figure 1. Morphology and elemental distribution of the precipitates obtained by STEM. (a) scanning transmission electron micrograph of sample "HAP_SrHAP"; (b-h) x-ray intensity maps showing the P/Sr, O/Sr, Ca/Sr elemental distribution ratios and the elemental distributions of Ca, P, O, and Sr respectively, all detected at the K-edge.

Figure 2. FTIR spectra for the reference solids $SrCO_3$ and FAP and for precipitates formed with the $SrCO_3$ seed template in the presence of F. Spectra are normalized to the baseline.

Figure 3. XANES obtained at the Ca-K-edge for (a) all precipitates with the references HAP and FAP, (b) zoom into the white-line for HAP_SrHAP, β-TCP_SrHAP, brushite_SrHAP, non-stoich_SrHAP and reference HAP, and (c) XANES obtained for all other calcium-phosphate references.

Figure 4. Spectra (background subtracted) obtained by EXAFS at the Ca-K-edge for (a) the reference solid HAP and precipitates formed using the SrHAP seed template in the absence of F and (b) the reference solid FAP and precipitates formed using SrHAP and $SrCO_3$ seed template in the presence of F.

Figure 5. X-ray diffractograms of (a) reference solids HAP and SrHAP compared with the precipitates formed using the seed template SrHAP in the absence of F, and (b) reference solids FAP and SrHAP with precipitates formed using the SrHAP seed template in the presence of F.

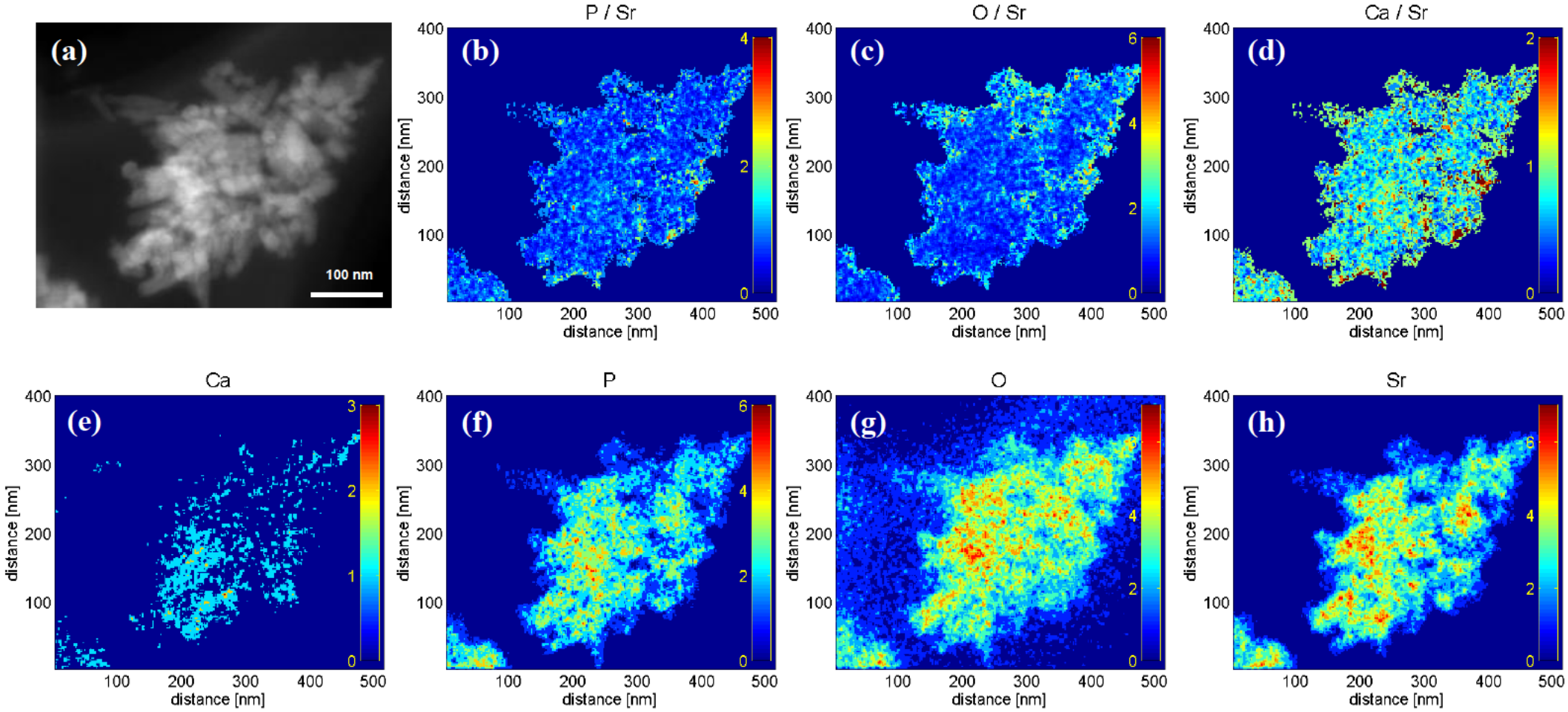
(a)
100 nm
P / Sr
(b)
O / Sr
(c)
Ca / Sr
(d)
Ca
(e)
P
(f)
O
(g)
Sr
(h)
distance [nm]
100
200
300
400
500

(Figure 1)

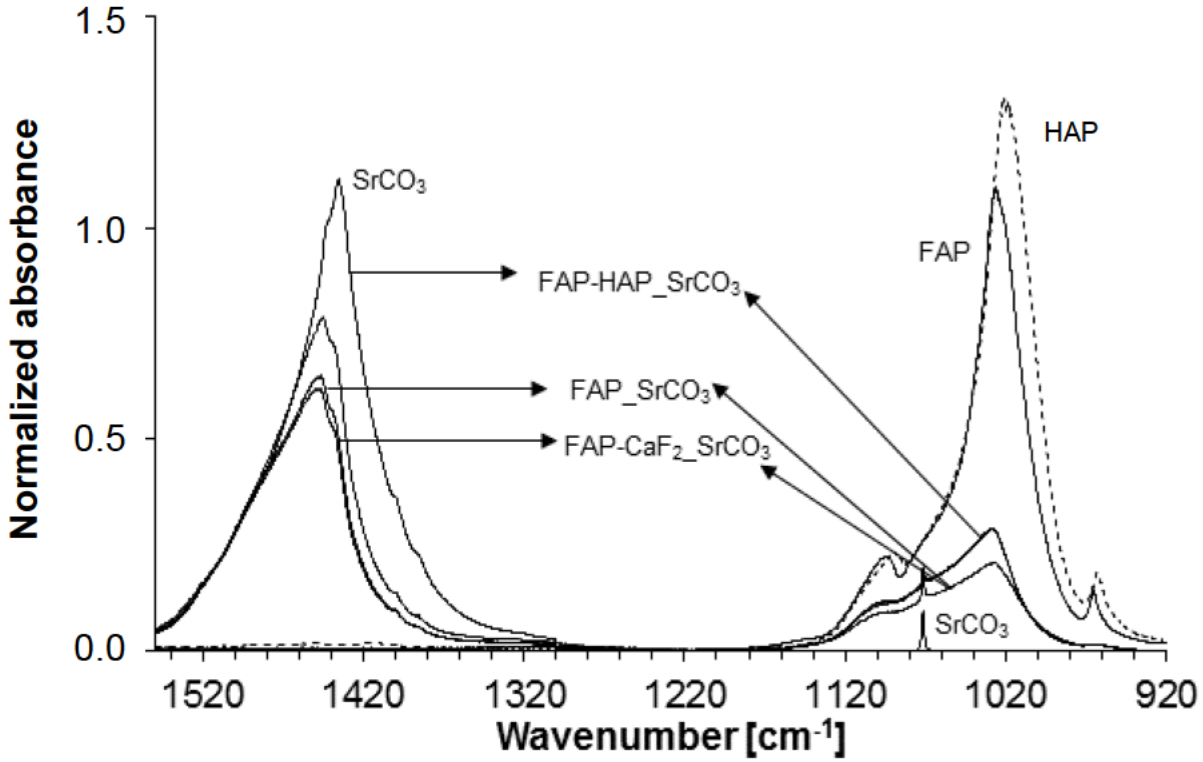
1.5
1.0
0.5
0.0
Normalized absorbance
SrCO3
HAP
FAP
FAP-HAP_SrCO3
FAP_SrCO3
FAP-CaF2_SrCO3
SrCO3
1520
1420
1320
1220
1120
1020
920
Wavenumber [cm-1]

(Figure 2)

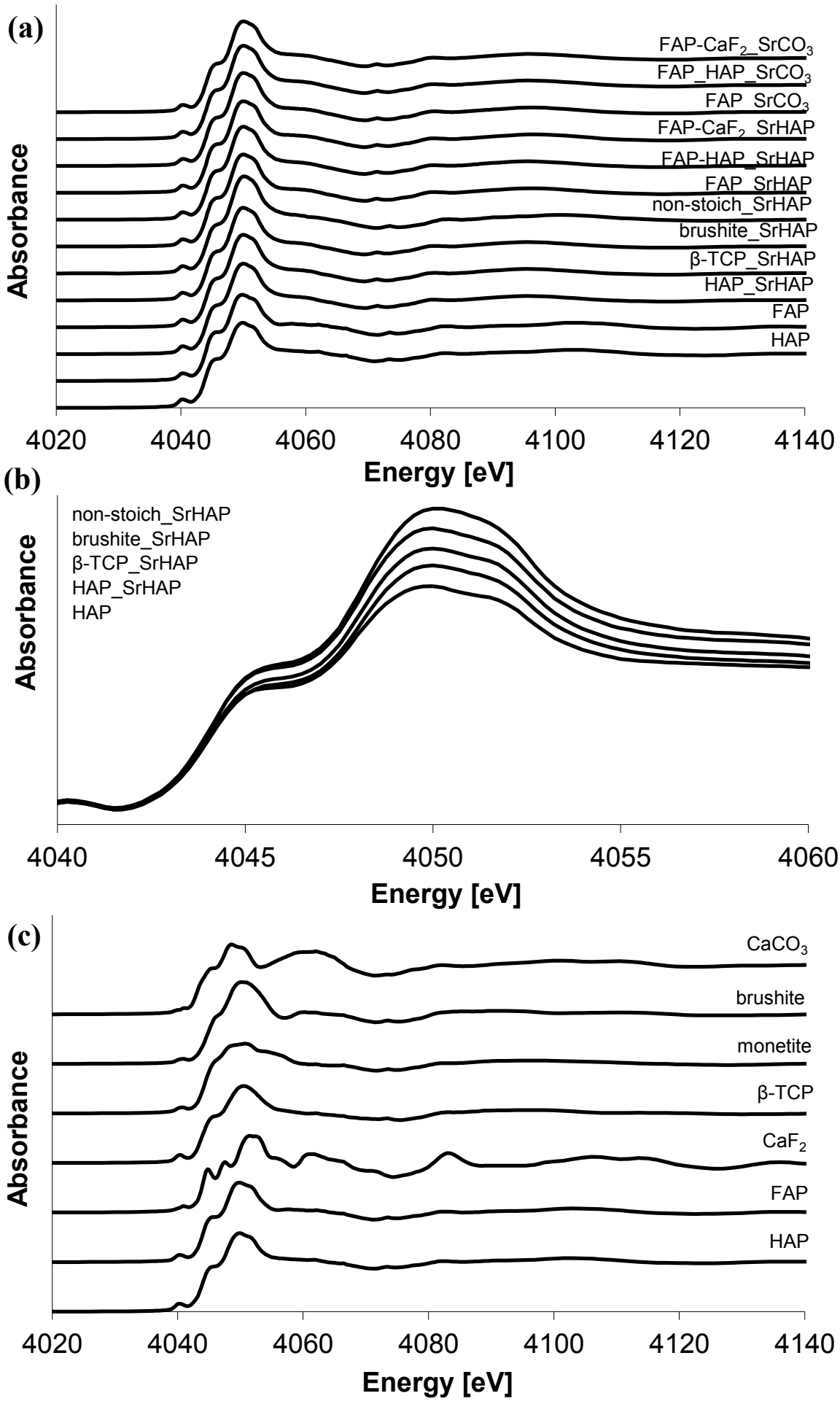
(a)
Absorbance
FAP-CaF2_SrCO3
FAP_HAP_SrCO3
FAP_SrCO3
FAP-CaF2_SrHAP
FAP-HAP_SrHAP
FAP_SrHAP
non-stoich_SrHAP
brushite_SrHAP
β-TCP_SrHAP
HAP_SrHAP
FAP
HAP
4020
4040
4060
4080
4100
4120
4140
Energy [eV]
(b)
Absorbance
non-stoich_SrHAP
brushite_SrHAP
β-TCP_SrHAP
HAP_SrHAP
HAP
4040
4045
4050
4055
4060
Energy [eV]
(c)
Absorbance
CaCO3
brushite
monetite
β-TCP
CaF2
FAP
HAP
4020
4040
4060
4080
4100
4120
4140
Energy [eV]

(Figure 3)

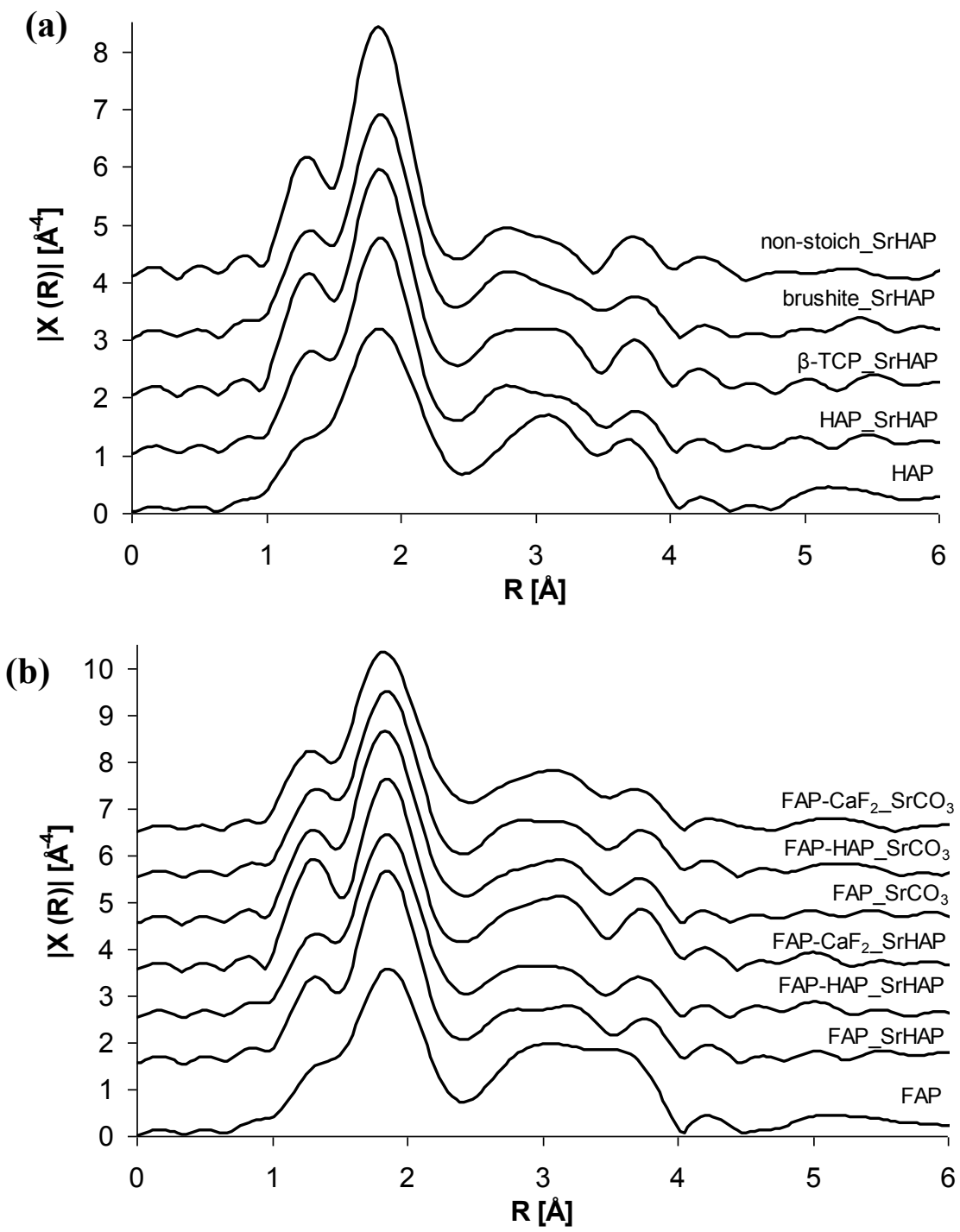
(a)
|X (R)| [Å-4]
R [Å]
non-stoich_SrHAP
brushite_SrHAP
β-TCP_SrHAP
HAP_SrHAP
HAP
(b)
|X (R)| [Å-4]
R [Å]
FAP-CaF2_SrCO3
FAP-HAP_SrCO3
FAP_SrCO3
FAP-CaF2_SrHAP
FAP-HAP_SrHAP
FAP_SrHAP
FAP

(Figure 4)

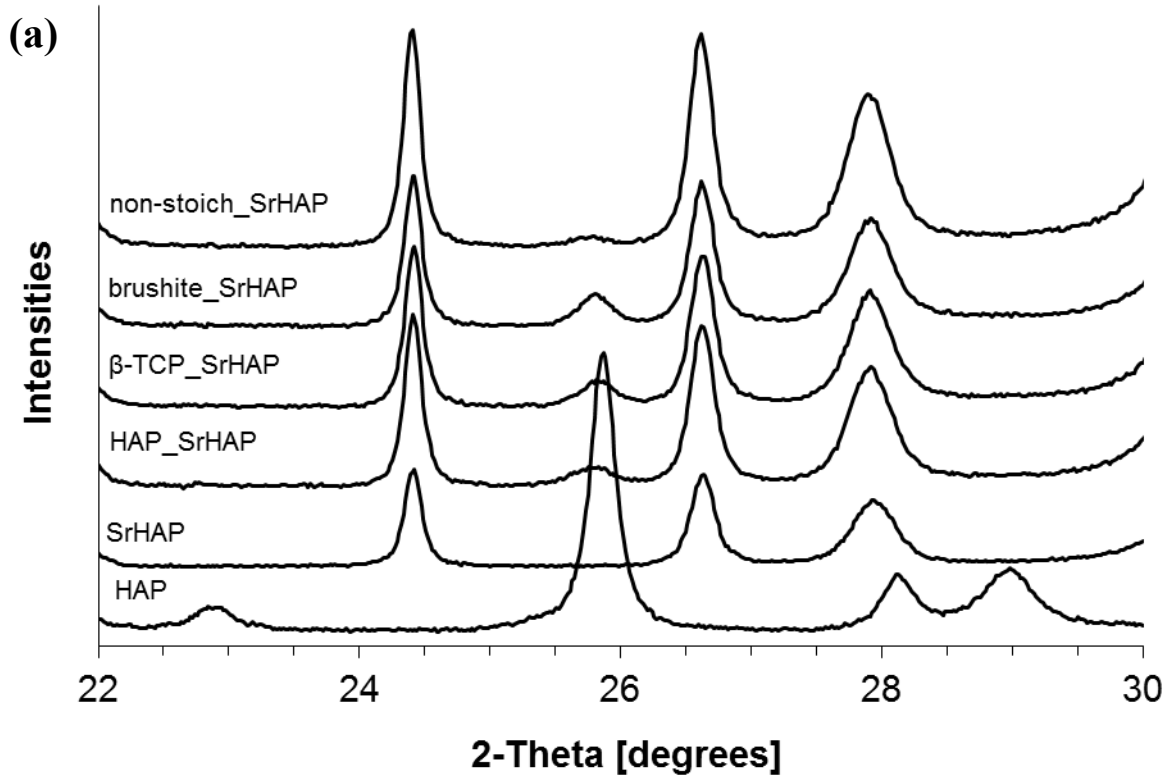
(a)
Intensities
non-stoich_SrHAP
brushite_SrHAP
β-TCP_SrHAP
HAP_SrHAP
SrHAP
HAP
22
24
26
28
30
2-Theta [degrees]

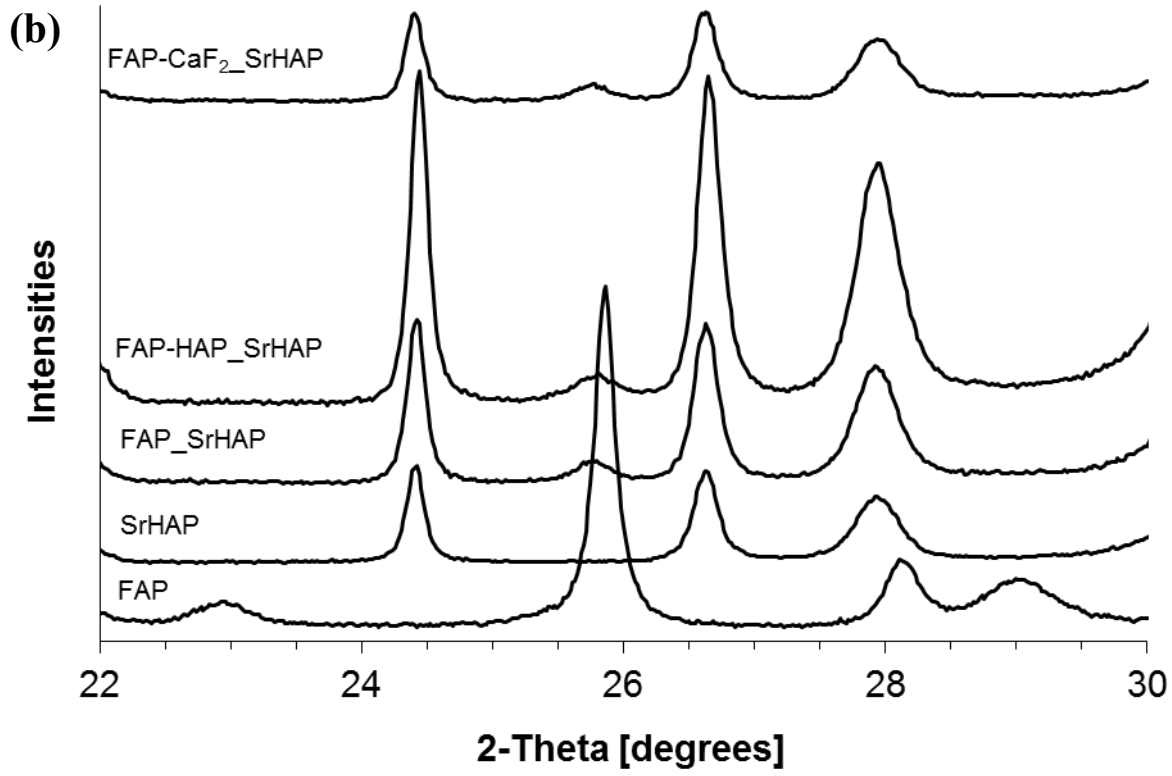
(b)
Intensities
FAP-CaF2_SrHAP
FAP-HAP_SrHAP
FAP_SrHAP
SrHAP
FAP
22
24
26
28
30
2-Theta [degrees]

(Figure 5)

Table 1. Summary of samples prepared with different Ca, PO_4 (and F) concentrations and seeding templates at pH 7.3.

Sample name	Seed	Added Ca:PO_4(:F) concentrations [mM]	Molar Ca/P		
			ideal[a]	added[b]	precipitate[c]
brushite_SrHP	SrHAP	5:5 stoichiometric for brushite	1.00	0.98	1.51
β-TCP_SrHAP	SrHAP	5:3.33 stoichiometric for β-TCP	1.50	1.44	1.46
HAP_SrHAP	SrHAP	5:3 stoichiometric for HAP	1.67	1.60	1.56
non-stoich_SrHAP	SrHAP	2:4 non-stoichiometric	-	0.48	1.16
FAP-CaF_2_SrHAP	SrHAP	6:3:3 PO_4-limited for FAP	-	1.97	1.90
FAP-CaF_2_$SrCO_3$	$SrCO_3$	6:3:3 PO_4-limited for FAP	-	2.00	1.71
FAP_SrHAP	SrHAP	5:3:1 stoichiometric for FAP	1.67	1.62	1.66
FAP_$SrCO_3$	$SrCO_3$	5:3:1 stoichiometric for FAP	1.67	1.67	1.49
FAP-HAP_SrHAP	SrHAP	5:3:0.5 F-limited for FAP	1.67	1.62	1.52
FAP-HAP_$SrCO_3$	$SrCO_3$	5:3:0.5 F-limited for FAP	1.67	1.67	1.49

[a] for solid shown as stoichiometric; [b] corrected for partial dissolution of SrHAP during 10min pre-equilibration; [c] based on the decrease in dissolved concentrations observed after 3 d; note: [b] and [c] are averaged values based on duplicate experiments.

Table 2. Surface composition obtained from XPS analysis. Data are shown [atm%] for references (HAP, FAP, SrHAP, $SrCO_3$ and CaF_2) and precipitates.

	O(1s)	F(1s)	Ca(2p)	P(2s) [b)]	Sr(3p)	C(1s)	(Sr+Ca)/P	Ca/P
HAP [a)]	61.90	0.00	23.80	14.30	-	ni		1.67
FAP [a)]	57.10	4.80	23.80	14.30	-	ni		1.67
CaF_2 [a)]	0.00	66.70	33.30	0.00	-	ni		
SrHAP [a)]	61.90	0.00	0.00	14.30	23.80	ni		
$SrCO_3$ [a)]	60.00	0.00	0.00	0.00	20.00	20.00		
HAP	65.70	0.00	20.20	14.10	-	ni		1.43
FAP	60.80	4.00	21.00	14.20	-	ni		1.47
CaF_2	0.00	63.70	36.30	0.00	-	ni		
SrHAP	59.23	0.30*	0.00	13.54	26.93	ni	1.99	
$SrCO_3$	57.39	0.55*	0.00	0.36	25.14	16.57	69.83	
HAP_SrHAP	60.17	0.47*	4.03	13.56	21.77	ni	1.90	0.30
β-TCP_SrHAP	61.35	0.45*	8.10	14.11	15.99	ni	1.71	0.57
brushite_SrHAP	61.55	0.52*	7.73	14.42	15.78	ni	1.63	0.54
non-stoich_SrHAP	61.82	0.30*	3.25	12.88	21.76	ni	1.94	0.25
FAP_SrHAP	59.89	0.97	3.30	14.14	21.71	ni	1.77	0.23
FAP-HAP_SrHAP	59.94	1.18	7.79	14.83	16.25	ni	1.62	0.53
FAP-CaF_2_SrHAP	58.89	2.98	5.28	14.16	18.69	ni	1.69	0.37
FAP_$SrCO_3$	56.79	2.62	7.95	7.40	15.09	10.16	3.11	1.07
FAP-HAP_$SrCO_3$	59.05	1.79	8.82	8.90	12.83	8.61	2.43	0.99
FAP-CaF_2_$SrCO_3$	54.57	4.58	10.27	8.46	12.65	9.48	2.71	1.21

[a] nominal values for example: HAP = 5Ca + 3P + 13O = 21atoms → 13O = 61.90 atm%; [b] P(2p) for HAP, FAP, CaF_2 as data originates from different analysis as the rest of the samples; (-): not detected; (ni): carbon (C1s) was not included in compositional data analysis, average C contamination was 1.23 ± 0.73 atm% (n = 7) in all SrHAP-based precipitates and was mainly attributed to C-C bonding and was therefore considered to be contamination. Samples of $SrCO_3$-based precipitates contained an average C content of 9.42 ± 0.78 atm% (n = 3), which was less than for the reference $SrCO_3$ sample (16.57 atm%) and was included in the data presentation as it was mainly attributed to C-O bonding. The signals of "FAP_SrHAP" and "FAP-CaF_2_SrHAP" did not exhibit sufficient intensity due to insufficient solid used for sample preparation. The detection limit is approximately 1.0 atm%. (*) F signals are artifacts, most probably due to contamination by sample preparation. The corresponding background F contamination of about 0.5 atm% was not subtracted from the values observed for solids precipitated in the experimental samples. All spectra were corrected for charging effects by setting the binding energy of C(1s) to 284.8 eV.